Optical hyperpolarization of nitrogen donor spins in bulk diamond

M. Loretz,[1] H. Takahashi,[1] T. F. Segawa,[1,2] J. M. Boss,[1] and C. L. Degen[1,*]
[1]*Department of Physics, ETH Zurich, Otto Stern Weg 1, 8093 Zurich, Switzerland*
[2]*Department of Chemistry and Applied Biosciences, ETH Zurich, Vladimir Prelog Weg 2, 8093 Zurich, Switzerland*
(Received 23 December 2016; published 14 February 2017)

We report hyperpolarization of the electronic spins associated with substitutional nitrogen defects in bulk diamond crystals. Hyperpolarization is achieved by optical pumping of nitrogen vacancy centers followed by rapid cross relaxation at the energy level matching condition in a 51 mT bias field. The maximum observed donor spin polarization is 0.9%, corresponding to an enhancement of 25 compared to the thermal Boltzmann polarization. A further accumulation of polarization is impeded by an anomalous optical saturation effect that we attribute to charge state conversion processes. Hyperpolarized nitrogen donors may form a useful resource for increasing the efficiency of diamond-based dynamic nuclear polarization devices.

DOI: 10.1103/PhysRevB.95.064413

I. INTRODUCTION

Nuclear magnetic resonance (NMR) spectroscopy is a powerful method for contemporary molecular characterization and diagnostics due to a superb spectroscopic resolution. By contrast, the sensitivity of NMR is low due to its reliance on the Boltzmann polarization, which is $P \leqslant 10^{-4}$ even for the highest fields accessible with state-of-the-art superconducting magnets [1,2]. The low sensitivity posits that a sufficiently large sample volume in high enough concentration is available, which presents a significant obstacle when delicate samples and nuclei with a low isotope abundance or low gyromagnetic ratio are involved. In order to circumvent the sensitivity limitations of NMR, hyperpolarization techniques that increase the polarization beyond the Boltzmann level—ideally approaching 100% polarization—are being widely explored. In particular, these include triplet dynamic nuclear polarization (DNP) [3], dissolution DNP [4,5], optically pumped noble gases [6–9] and semiconductors [10–12], and many varieties of those techniques [13,14]. The main drawbacks of most hyperpolarization methods are a cost-prohibitive cryogenic hardware and an often-limited area of application.

A new concept for an inexpensive, room-temperature polarizer is based on diamond crystals doped with nitrogen-vacancy defects (NV centers) [15–19]. In a diamond polarizer, hyperpolarization is induced by optical pumping of NV defect spins using intense laser illumination. Diamond polarizers are proposed to have many advantages, which include, beside room-temperature compatibility, a rapid optical pumping, near-unity polarization, and no need for sample doping by radicals. In addition, the chemical inertness and stability of diamond make the device potentially reusable for a large variety of liquid samples. The central bottleneck of diamond polarizers, however, is the transport of polarization from the defect spins within diamond to target spins outside of diamond. To date, this step has been demonstrated indirectly and on a few-spin scale [20–22]. Because the separation between source and target nuclear spins must be less than ∼5 nm, only defect centers located in the top surface layer contribute to the transfer. Thus, even for high NV densities of order 10^{18} cm^{-3} (∼10 ppm) [23] the number of actively participating spins is low. One proposed remedy is to structure the surface so as to increase its effective surface area [18].

Another potential route for increasing hyperpolarization efficiency, explored here, takes advantage of abundant substitutional nitrogen defects (P1 centers) [24,25]. Rather than directly polarizing an outside analyte, the polarization is first transferred to a large bath of nitrogen donor spins using a cross-relaxation process (see Fig. 1). Since P1 centers can approach densities of 10^{20} cm^{-3} (∼400 ppm) [23], the electronic spin polarization at the diamond surface can potentially be greatly increased. In addition, because P1 centers, in contrast to NV centers, do not require a preferential alignment with the external bias field, they are more suited for transferring polarization to outside nuclear spins.

In this paper, we investigate the hyperpolarization of nitrogen donor spins in bulk diamond by *in situ* electron paramagnetic resonance (EPR) spectroscopy. The hyperpolarization is induced by optical pumping of NV centers and cross relaxation at the energy level matching of the two spin species at $B = 51$ mT [see Fig. 1(b)]. We observe that large polarization enhancement factors, exceeding 100 for NV centers and up to 25 for P1 centers, can be generated. In addition, we observe that the polarization enhancement unexpectedly saturates already at very low laser intensities, and far below the known saturation intensity for NV centers. By comparing the results to a kinetic model of spin populations, we find that the anomalous saturation can be partially explained by charge state conversions of NV and P1 defects.

II. EXPERIMENT

Experiments are carried out on a home-built EPR spectrometer specifically designed for operation at 51 mT. The EPR probe consists of an inductively coupled loop gap resonator resonant at 1.44 MHz with a quality factor of 1500 [30,31]. The magnetic field is provided by a pair of permanent disk magnets arranged in a Helmholtz configuration and an additional Helmholtz coil with a sweep range of 4 mT. In order to orient the magnetic field along one of the ⟨111⟩ diamond crystal axes, magnets and coil are oriented such that the center axis of the Helmholtz pair is at an angle of 55° from the (100) surface normal of a diamond chip (see Fig. S1 in the Supplemental

*degenc@ethz.ch

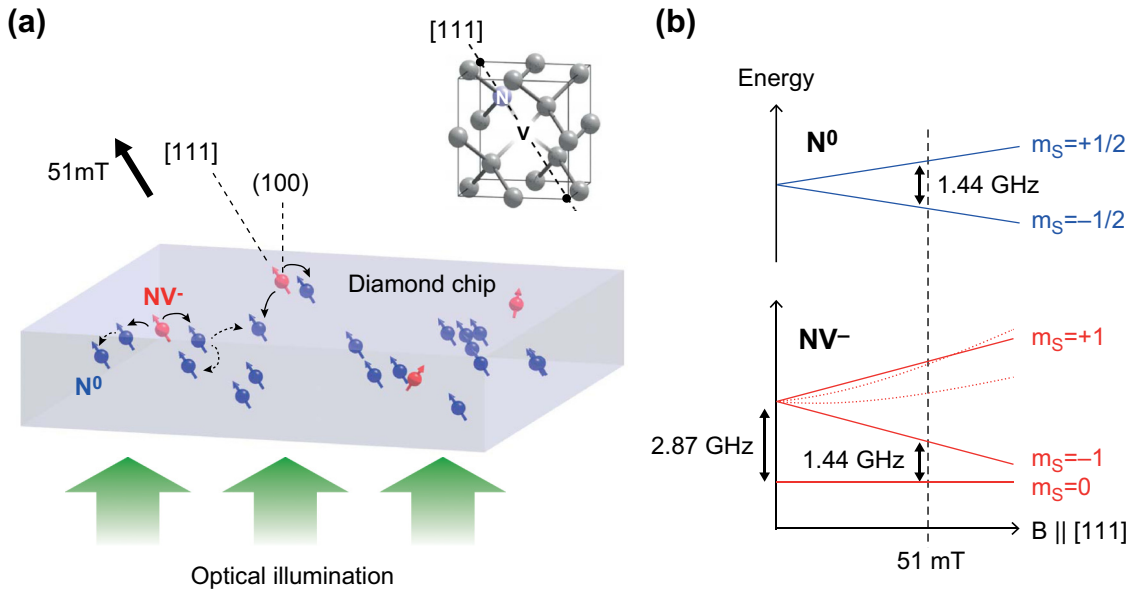

FIG. 1. (a) Basic arrangement for optical hyperpolarization of nitrogen donor spins in diamond. First, nitrogen vacancy centers (NV^-, red, spin $S = 1$) are optically polarized into the $m_S = 0$ spin state by exposure to a green laser beam [26]. Next, the polarization is transferred to adjacent nitrogen defects (N^0, blue, spin $S = \frac{1}{2}$) using cross relaxation mediated by the dipolar interaction (solid arrows). Only those NV^- centers whose N-V symmetry axis is aligned with the external bias field (see inset) are optically pumped and contribute to cross relaxation. Finally, the polarization is rapidly distributed in the nitrogen spin bath via spin diffusion (dashed arrows). The polarization may later be transferred to target nuclear spins outside the diamond chip. This could be achieved either directly, using the integrated solid effect [27] or the Overhauser effect [28], or indirectly, via additional spin labels on the diamond surface [29] or in the analyte. (b) Spin energy level diagram indicating the matching condition between the $m_S = 0 \leftrightarrow m_S = -1$ transition of aligned NV^- spins and the $m_S = -\frac{1}{2} \leftrightarrow m_S = +\frac{1}{2}$ transition of N^0 at 51 mT. The matching occurs when the Zeeman field is exactly one half of the NV^- crystal field (dashed line). Dotted curves indicate the transitions of NV^- spins not aligned with the magnetic field.

Material [32]). The diamond crystal is then rotated around [100] until the magnetic field becomes parallel to [111]. This second alignment is performed by minimizing the EPR frequency of the $m_S = 0 \leftrightarrow m_S = -1$ transition as the sample is being rotated. EPR spectra are acquired with a standard continuous-wave detection scheme with a field modulation of 9.7 kHz and a low microwave power of a few 100 nW. To optically pump the NV centers, a laser beam is directed through an opening along the longitudinal direction of the resonator and onto the flat (100) surface of the diamond chip. The laser beam has a diameter of ∼5 mm corresponding to an intensity of ∼50 mW/mm^2 for 1 W of incident light. The optical beam is generated by a 532 nm cw laser (Coherent Verdi 10 W) and gated by a shutter. To mitigate the absorptive heating, the diamond chip is exposed to a flow of cold nitrogen gas (∼200 K) via a central sample tube.

Two diamond chips are used in this study. Both chips are grown by high-pressure, high-temperature synthesis and are of type Ib (ElementSix Ltd.). The chips have exposed {100} surfaces and lateral dimensions of 3 × 3 mm^2 and thicknesses of 0.3 mm (chip A) and 0.08 mm (chip B), respectively. To increase the NV density, chip A (chip B) is irradiated by a 2 MeV electron beam (Leoni Studer AG) for a total duration of 30 h (40 h) with an intermediate annealing step after 10 h (20 h) and a final annealing step at the end. Annealing is performed in high vacuum and at 850 °C for 2 h [23,33]. A wide-field fluorescence measurement is used to confirm that the NV density is uniform over the chip surface. Defect densities of the relevant NV^- and N^0 charge states are quantified by cw EPR spectroscopy on a Bruker ElexSys E500 X-Band (9.855 GHz) spectrometer by comparing the double-integrated signal intensities with a standard sample (see Fig. S2). Defect densities are $[N^0] = 77$ ppm and $[NV^-] = 9$ ppm for chip A and $[N^0] = 36$ ppm and $[NV^-] = 11$ ppm for chip B (see Table I) with an uncertainty of 20%.

III. RESULTS

A. EPR spectroscopy at 51 mT

Figure 2 shows two representative EPR spectra recorded with the home-built setup at 51 mT in the absence and presence of green laser illumination. Without illumination, the spectrum shows the typical pattern of five resonances centered around 1452 MHz caused by the center and ^{14}N hyperfine satellite transitions of N^0 [Fig. 2(a)] [25]. The NV^- resonance is not visible in this spectrum because the Boltzmann polarization is too low to produce a detectable signal at these low concentrations.

Under optical illumination with 300 mW, the $m_S = 0 \leftrightarrow m_S = -1$ resonance of the NV^- signal becomes visible at ∼1440 MHz [see Fig. 2(b)]. In addition, the five N^0 resonances are strongly enhanced. A control experiment (Fig. S2) shows that the N^0 signal enhancement does not occur at the X band. This demonstrates that the cross-relaxation mechanism is effective only near 51 mT, as expected. Despite the fact that the level matching condition is only fulfilled for the central N^0 resonance, a similar polarization enhancement is observed for all four hyperfine-shifted N^0 resonances, probably because

TABLE I. Important quantities for the measurements in Fig. 2. Effective NV^- density and polarizations refer to the ~25% of NV centers whose symmetry axes are aligned with the bias field. Boltzmann polarization is reported for 200 K.

Defect	Charge state	Spin	Density	Effective density	Polarization (Boltzmann)	Polarization (300 mW)	Enhancement
NV	NV^-	$S = 1$	9 ppm	2.3 ppm	0.034%	3.5%	103
P1	N^0	$S = \frac{1}{2}$	77 ppm	77 ppm	0.034%	0.86%	25

of spectral diffusion due to nuclear spin flips. To evaluate the polarization enhancement, we can fit each resonance by the derivative of a Gaussian function and subsequently double integrate and add all resonances. For the nonilluminated spectrum, the integrated signal intensity is 11 a.u. for N^0. Considering the proportions of defect densities (Table I), the corresponding NV^- intensity is estimated at 0.32 a.u. Under optical illumination, the signal intensities are 280 a.u. for N^0 and 33 a.u. for NV^-. The corresponding polarization enhancement is therefore about 100 and 25, respectively (see Table I). Because the signal in the nonilluminated reference spectrum is small, the uncertainty in these enhancement factors is rather large, on the order of 25% [2 standard deviation (s.d.)].

To investigate the maximum possible polarization enhancement, we measure the induced spin polarizations as a function of laser power. Figure 3 plots the spin polarization for NV^- and N^0 versus laser intensity. The spin polarization is calculated by comparing the EPR signal intensities to the reference values from Table I. The laser intensity I represents an effective intensity because the deeper regions of the diamond chips receive less light due to optical absorption; the reduction compared to the incident intensity is approximately 0.50 for chip A and 0.73 for chip B, respectively, as inferred from the absorption cross section of the NV^- center ($\sigma = 3 \times 10^{-17}$ cm^2 [34]) and the chip thicknesses. Figure 3 shows that at low laser intensities, $I \lesssim 4$ mW/mm^2, the observed spin polarization increases proportionally with the optical power. This behavior is expected in the regime where the optical pump rate k_0 is slower than the spin relaxation rate $\Gamma_{NV^-} = (T_{1,NV^-})^{-1}$. The pump rate can be estimated from the absorption cross section of the NV^- center and is about $k_0 = 8 \times 10^3$ s$^{-1} \times I/[\mathrm{W\,mm^{-2}}]$ [34]. This yields $k_0 \approx 32$ s^{-1} for $I = 4$ mW/mm^2 (see the upper scale in Fig. 3), which is indeed below the expected spin relaxation rate of $\Gamma_{NV^-} \sim 50$ s^{-1} [35].

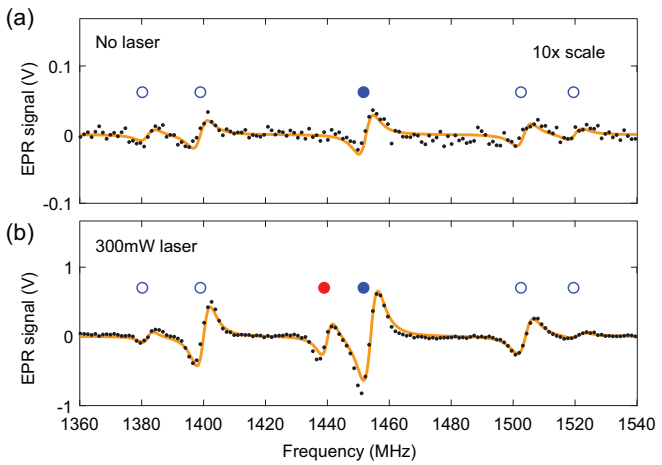

FIG. 2. (a) EPR spectrum at 51 mT of diamond chip A with no laser illumination. Five N^0 resonances are visible, including the central transition (solid blue circle) and the four hyperfine-shifted transitions (open blue circles) associated with the $I = 1$ nitrogen ^{14}N nuclear spin. The NV^- resonance is below the detection limit. (b) EPR spectrum with 300 mW laser illumination. The $m_S = 0 \leftrightarrow m_S = -1$ transition of aligned NV^- centers appears as an additional peak at ~1440 MHz (solid red circle); other NV^- resonances fall outside of the spectral range (see Fig. S3). A strong polarization enhancement is observed for both NV^- and N^0. Solid lines are fits. Spectra are recorded in a single passage with a dwell time of about 1 s per point. Units have been converted from field to frequency using the free-electron g factor. Additional quantities are given in Table I.

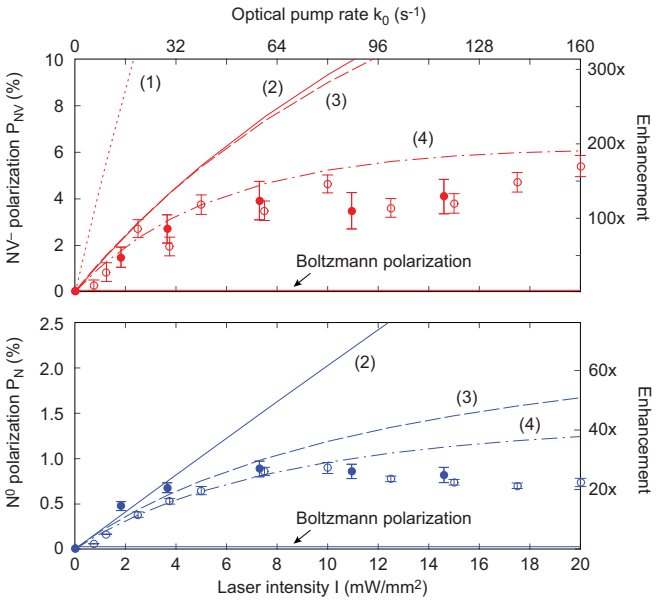

FIG. 3. Spin polarization of NV^- and N^0 plotted as a function of laser intensity. The corresponding laser powers are 0–800 mW. Open circles represent chip A and solid circles represent chip B. The maximum observed polarization enhancement is 170 for NV^- and 25 for N^0. Solid and dashed lines represent the different kinetic models discussed in the main text: (1) No cross relaxation, $P_{NV^-} = k_0/[k_0 + 3\Gamma_{NV^-}]$, (2) simple cross relaxation, (3) cross relaxation and $N^0 \leftrightarrow N^+$ charge state conversion, and (4) cross relaxation and $N^0 \leftrightarrow N^+$, $NV^- \leftrightarrow NV^0$ charge state conversions. An anomalous saturation effect is observed for laser intensities above ca. 10 mW/mm^2 which is not explained by the models. Model parameters are given in Table II and are for chip A; the slight deviation of the chip B data for the N^0 panel is due to the different NV^- concentration. Error bars are fit errors (2 s.d.).

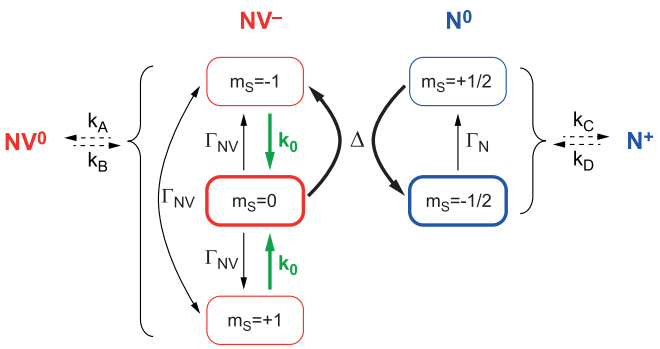

FIG. 4. Reservoir model of the NV-P1 system. Green bold arrows indicate the pumping process, black bold arrows indicate rapid cross relaxation, and bold boxes represent majority populations. Dashed arrows indicate charge state conversions. Solid arrows indicate the principal direction of population flow. Rate constants are explained in the text.

By contrast, at laser intensities above 10 mW/mm^2, the polarization saturates and does not exceed ∼5% for NV$^-$ and ∼0.9% for N^0, respectively. This saturation is unexpected because the optical intensity is orders of magnitude below the optical saturation limit for NV$^-$ centers (∼10^3 W/mm^2) [36]. The saturation observed in Fig. 3 is therefore not related to a simple electronic excitation of the NV center and must be caused by another mechanism. A similar anomalous saturation has recently been reported in an EPR study by Drake *et al.* [15], which was carried out at the *X* band at 9.7 GHz where cross relaxation can be neglected. Drake *et al.* observed an "anomalous" saturation of the EPR signal for laser intensities between 10 and 20 mW/mm^2, in good agreement with our finding. The authors hypothesized that increased relaxation and NV$^-$ photoionization could cause this effect. In the following, we argue, based on a simple kinetic model, that the anomalous saturation involves photoionization of both NV$^-$ and N^0 and is likely assisted by other charge traps in the host crystal. Relaxation itself, by contrast, does not appear to be the leading cause for the saturation effect.

B. Modeling of polarization dynamics including cross relaxation

We have analyzed the polarization buildup in terms of population dynamics between coupled spin baths (see Fig. 4). The most basic model takes into account longitudinal spin relaxation rates Γ_{NV^-} and Γ_{N^0} for NV$^-$ and N^0, respectively, and a pairwise cross-relaxation rate Δ between the reservoirs. Later on we will extend the model to also include charge state conversions to neutral NV^0 and positive N$^+$, respectively.

First, we can inspect the buildup of polarization in the absence of charge state conversion processes. The dynamics of the spin populations are then described by the following set of rate equations,

$$\frac{dp_{\mathrm{NV}^-_{-1}}}{dt} = -k_0 p_{\mathrm{NV}^-_{-1}} + \Gamma_{NV^-}\left(-2p_{\mathrm{NV}^-_{-1}} + p_{\mathrm{NV}^-_{0}} + p_{\mathrm{NV}^-_{+1}}\right) - R\Delta\left(p_{\mathrm{NV}^-_{-1}} p_{\mathrm{N}^0_{-1/2}} - p_{\mathrm{NV}^-_{0}} p_{\mathrm{N}^0_{+1/2}}\right), \quad (1)$$

TABLE II. Parameters used for the model curves in Fig. 3. Γ_{NV^-} and Γ_{N^0} values were chosen such that the model best reproduced the low intensity ($I < 4$ mW/m^2) part of the data. We note that these values are in excellent agreement with reported rates at 200 K temperature [35,42]. Δ is estimated ∼1 MHz based on the dipolar coupling between nearest-neighbor spins. k_0 is according to the text. k_A and k_C represent upper bounds [37,39]. k_B and k_D represent the values that led to the best agreement between model and experiment. *R* is the ratio of effective densities in Table I. Parameters are for diamond chip A.

Parameter	NV center	P1 center
Spin relaxation rates Γ_{NV^-} and Γ_{N^0}	55 s^{-1}	55 s^{-1}
Cross-relaxation rate Δ	>10^5 s^{-1}	
Optical pump rate k_0	0–160 s^{-1}	–
Ionization rate k_A and k_C	k_0	
Recombination rate k_B and k_D	10^3 s^{-1}	
Ratio of spin reservoirs	$R \approx 34$	

$$\frac{dp_{\mathrm{NV}^-_{0}}}{dt} = +k_0\left(p_{\mathrm{NV}^-_{-1}} + p_{\mathrm{NV}^-_{+1}}\right) + \Gamma_{NV^-}\left(-2p_{\mathrm{NV}^-_{0}} + p_{\mathrm{NV}^-_{-1}} + p_{\mathrm{NV}^-_{+1}}\right) + R\Delta\left(p_{\mathrm{NV}^-_{-1}} p_{\mathrm{N}^0_{-1/2}} - p_{\mathrm{NV}^-_{0}} p_{\mathrm{N}^0_{+1/2}}\right), \quad (2)$$

$$\frac{dp_{\mathrm{NV}^-_{+1}}}{dt} = -k_0 p_{\mathrm{NV}^-_{+1}} + \Gamma_{NV^-}\left(-2p_{\mathrm{NV}^-_{+1}} + p_{\mathrm{NV}^-_{-1}} + p_{\mathrm{NV}^-_{0}}\right), \quad (3)$$

$$\frac{dp_{\mathrm{N}^0_{-1/2}}}{dt} = -\Gamma_{N^0}\left(p_{\mathrm{N}^0_{-1/2}} - p_{\mathrm{N}^0_{+1/2}}\right) - \Delta\left(p_{\mathrm{NV}^-_{-1}} p_{\mathrm{N}^0_{-1/2}} - p_{\mathrm{NV}^-_{0}} p_{\mathrm{N}^0_{+1/2}}\right), \quad (4)$$

$$\frac{dp_{\mathrm{N}^0_{+1/2}}}{dt} = -\Gamma_{N^0}\left(-p_{\mathrm{N}^0_{-1/2}} + p_{\mathrm{N}^0_{+1/2}}\right) + \Delta\left(p_{\mathrm{NV}^-_{-1}} p_{\mathrm{N}^0_{-1/2}} - p_{\mathrm{NV}^-_{0}} p_{\mathrm{N}^0_{+1/2}}\right), \quad (5)$$

where $p_{\mathrm{NV}^-_{-1}}$, $p_{\mathrm{NV}^-_{0}}$, and $p_{\mathrm{NV}^-_{+1}}$ denote the relative populations (probabilities) of the three $\mathrm{NV}^-_{m_S}$ spin states and $p_{\mathrm{N}^0_{-1/2}}, p_{\mathrm{N}^0_{+1/2}}$ denote the relative populations of the two $\mathrm{N}^0_{m_S}$ spin states. The constant $R = [\mathrm{N}^0]/(0.25[\mathrm{NV}^-])$ is the ratio between the sizes of the N^0 and effective NV$^-$ spin baths (see Table II). Note that we assume equal spin relaxation rates between all three NV$^-$ spin levels. Although the relaxation between the $m_S = \pm 1$ states is likely much slower, the assumption of equal relaxation rates allows for a simple analysis. We verified through numerical simulations that the assumption only has a minor effect on the overall result.

We have resolved this model to calculate the equilibrium polarizations in the limit of fast cross relaxation ($\Delta \gg \Gamma_{NV^-}, \Gamma_{N^0}, k_0$). The polarizations are

$$P_{NV^-} = p_{\mathrm{NV}^-_{0}} - \frac{1}{2}\left(p_{\mathrm{NV}^-_{-1}} + p_{\mathrm{NV}^-_{+1}}\right) = \frac{k_0(2k_0 + R\Gamma_{N^0} + 4\Gamma_{NV^-})}{(k_0 + 2R\Gamma_{N^0} + 2\Gamma_{NV^-})(2k_0 + 6\Gamma_{NV^-})}, \quad (6)$$

$$P_{N^0} = p_{\mathrm{N}^0_{+1/2}} - p_{\mathrm{N}^0_{-1/2}} = \frac{k_0}{k_0 + 2R\Gamma_{N^0} + 2\Gamma_{NV^-}}. \quad (7)$$

Equations (6) and (7) are plotted as solid lines (curve 2) alongside the experimental data in Fig. 3 for the parameters given in Table II. We find that the model well describes the polarization enhancement of both spin species at low laser intensities, but that it cannot account for the saturation observed for intensities above roughly 10 mW/mm^2.

C. Modeling of polarization dynamics including charge state conversions

As a second step, we have analyzed whether charge state conversions between NV^- and neutral NV^0 as well as between N^0 and ionized N^+, which are known to be promoted by laser illumination [37,38], can be responsible for the anomalous saturation. Charge state conversions work to reduce the absolute EPR signal intensity through two effects: First, a significant conversion to NV^0 and N^+ decreases the sizes of the NV^- and N^0 spin reservoirs. Second, as charge interconversions are typically not spin preserving, they lead to accelerated spin relaxation.

In order to include charge state conversions, we extend our model by four additional rate equations, accounting for an ionization and a recombination process for each defect species. Several mechanisms are known to induce ionization or recombination. For the NV center, the best understood mechanisms include two-photon absorption processes that are able to cycle between NV^- and NV^0 [36,37,39]. Two-photon processes can, however, be neglected in our study because the laser intensity is very low. Photoconversion at low light levels is much less understood; in the following, we assume that electron loss occurs via tunneling from a photoexcited NV^- to a nearby N^+ and that recombination occurs through electron capture from the conduction band [37]. For P1 centers, the charge conversion typically occurs via a simple one-photon ionization and recombination process [40,41]. The four rate equations are then given by

$$\frac{dp_{\mathrm{NV}^-_j}}{dt} = -R' k_A p_{\mathrm{NV}^-_j} p_{\mathrm{N}^+} + \frac{1}{3} k_B n p_{\mathrm{NV}^0}, \tag{8}$$

$$\frac{dp_{\mathrm{NV}^0}}{dt} = +R' k_A p_{\mathrm{NV}^-} p_{\mathrm{N}^+} - k_B n p_{\mathrm{NV}^0}, \tag{9}$$

$$\frac{dp_{\mathrm{N}^0_j}}{dt} = -k_C p_{\mathrm{N}^0_j} + k_D n p_{\mathrm{N}^+} + \frac{1}{2} k_A p_{\mathrm{NV}^-} p_{\mathrm{N}^+}, \tag{10}$$

$$\frac{dp_{\mathrm{N}^+}}{dt} = +k_C p_{\mathrm{N}^0} - k_D n p_{\mathrm{N}^+} - k_A p_{\mathrm{NV}^-} p_{\mathrm{N}^+}, \tag{11}$$

where k_A through k_D are rate constants and $R' = [\mathrm{N}^0]/[\mathrm{NV}^-] = R/4$ (because all NV orientations participate in charge transfer). The subscript j indicates the respective spin state where $p_{\mathrm{NV}^-} = p_{\mathrm{NV}^-_{-1}} + p_{\mathrm{NV}^-_0} + p_{\mathrm{NV}^-_{+1}}$ and $p_{\mathrm{N}^0} = p_{\mathrm{N}^0_{-1/2}} + p_{\mathrm{N}^0_{+1/2}}$. Rates k_A and k_C describe photoexcitations and are therefore proportional to the pump rate k_0. k_B and k_D represent charge recombinations that are proportional to the concentration of conduction electrons n. If we stay within our simple model, neutrality of charge requires that n is given by $n = R' p_{\mathrm{N}^+} - p_{\mathrm{NV}^-}$, where n is normalized by $[\mathrm{NV}_{\mathrm{tot}}]$.

We numerically evaluate the extended model described by Eqs. (1)–(11) using the Euler method for two situations. A first case only takes $N^0 \leftrightarrow N^+$ charge state conversions into account but neglects $NV^- \leftrightarrow NV^0$ ($k_A = k_B = 0$). The second scenario includes both types of charge state conversions. Because the rate constants k_A through k_D are not well known, we have tried a number of different parameter settings in order to best match the model to our data. The best effort result is given in Table II and the corresponding model curves are plotted as curves 3 and 4 in Fig. 3. We find that the extended model visibly improves the agreement with the experiment, and that both charge state conversion processes must be included to obtain a satisfactory agreement (curve 4). An inspection of the individual populations (Fig. S4) shows that the leading cause for the polarization saturation is a reduced concentration of NV^- and N^0.

Despite the qualitative agreement, a significant discrepancy clearly remains for laser intensities above 10 mW/mm^2. In addition, the typical electron concentration predicted by our model is high, of order $n[\mathrm{NV}_{\mathrm{tot}}] \sim 10^6\ \mu\mathrm{m}^{-3}$, which is several orders of magnitude larger than the values discussed in recent work of Jayakumar *et al.* [41]. Likewise, our charge recombination rates are several orders of magnitude slower. We note that both effects could be accounted for by deep trap states formed by additional defects in the diamond crystals. These trap states would act as sinks and reduce the density of conduction electrons n. This would slow down the recombination processes and decrease the concentrations of NV^- and N^0. In order to be effective, the trap states would need to lie far below the conduction band so that they cannot be directly excited by green laser illumination. There are several defects that could act as such trap states, such as divacancies formed during electron irradiation [43]. Additional evidence for a trap state hypothesis comes through recent photoconductivity measurements made by Chen *et al.* [44]. There, an unexpected quenching of pulsed photocurrents by low-intensity laser illumination was observed. The authors suggested a similar trap state model that slowly depleted the N^0 reservoir. Chen *et al.* also observed that short, intense laser pulses could replenish the N^0 reservoir. Pulsed laser excitation may therefore provide a means for also mitigating the anomalous saturation effect.

IV. CONCLUSIONS AND OUTLOOK

In conclusion, we have demonstrated a method for polarizing nitrogen donors in bulk diamond through optical pumping of NV centers and cross relaxation. The polarization transfer between NV centers and nitrogen donors was found to be very efficient when operating at the energy level matching condition at 51 mT. The maximum nitrogen donor polarization was 0.9%, corresponding to a gain of 25 over the Boltzmann polarization. The polarization enhancement saturated for an unexpectedly low illumination intensity of ~10 mW/mm^2, probably due to charge state conversion processes. Overcoming this anomalous saturation will be crucial for realizing diamond polarizer devices for dynamic nuclear polarization.

ACKNOWLEDGMENTS

The authors thank G. Jeschke for access to the X-band spectrometer. T.F.S. acknowledges Society in Science, The Branco Weiss Fellowship, administered by the Eidgenossische Technische Hochschule Zurich.

[1] K. Hashi, S. Ohki, S. Matsumoto, G. Nishijima, A. Goto, K. Deguchi, K. Yamada, T. Noguchi, S. Sakai, M. Takahashi, Y. Yanagisawa, S. Iguchi, T. Yamazaki, H. Maeda, R. Tanaka, T. Nemoto, H. Suematsu, T. Miki, K. Saito, and T. Shimizu, J. Magn. Reson. **256**, 30 (2015).

[2] https://www.bruker.com/products/mr/nmr/magnets/magnets/aeon-1ghz/overview.html, retrieved 2016/12/17.

[3] A. Henstra, T. S. Lin, J. Schmidt, and W. T. Wenckebach, Chem. Phys. Lett. **165**, 6 (1990).

[4] J. H. Ardenkjaer-Larsen, B. Fridlund, A. Gram, G. Hansson, L. Hansson, M. H. Lerche, R. Servin, M. Thaning, and K. Golman, Proc. Natl. Acad. Sci. USA **100**, 10158 (2003).

[5] D. Gajan, A. Bornet, B. Vuichoud, J. Milani, R. Melzi, H. A. van Kalkeren, L. Veyre, C. Thieuleux, M. P. Conley, W. R. Gruning, M. Schwarzwalder, A. Lesage, C. Coperet, G. Bodenhausen, L. Emsley, and S. Jannin, Proc. Natl. Acad. Sci. USA **111**, 14693 (2014).

[6] B. C. Grover, Phys. Rev. Lett. **40**, 391 (1978).

[7] N. D. Bhaskar, W. Happer, and T. McClelland, Phys. Rev. Lett. **49**, 25 (1982).

[8] B. M. Goodson, J. Magn. Reson. **155**, 157 (2002).

[9] D. M. L. Lilburn, G. E. Pavlovskaya, and T. Meersmann, J. Magn. Reson. **229**, 173 (2013).

[10] G. Lampel, Phys. Rev. Lett. **20**, 491 (1968).

[11] R. Tycko and J. A. Reimer, J. Phys. Chem. **100**, 13240 (1996).

[12] R. Tycko, Solid State Nucl. Magn. Reson. **11**, 1 (1998).

[13] R. G. Griffin and T. F. Prisner, Phys. Chem. Chem. Phys. **12**, 5737 (2010).

[14] J. A. Reimer, Solid State Nucl. Magn. Reson. **37**, 3 (2010).

[15] M. Drake, E. Scott, and J. A. Reimer, New J. Phys. **18**, 013011 (2016).

[16] R. Fischer, C. O. Bretschneider, P. London, D. Budker, D. Gershoni, and L. Frydman, Phys. Rev. Lett. **111**, 057601 (2013).

[17] J. Scheuer, I. Schwartz, Q. Chen, D. Schulze-Sunninghausen, P. Carl, P. Hofer, A. Retzker, H. Sumiya, J. Isoya, B. Luy, M. B. Plenio, B. Naydenov, and F. Jelezko, New J. Phys. **18**, 013040 (2016).

[18] D. Abrams, M. E. Trusheim, D. R. Englund, M. D. Shattuck, and C. A. Meriles, Nano Lett. **14**, 2471 (2014).

[19] J. P. King, K. H. Jeong, C. C. Vassiliou, C. S. Shin, R. H. Page, C. E. Avalos, H. J. Wang, and A. Pines, Nat. Commun. **6**, 8965 (2015).

[20] H. J. Mamin, M. Kim, M. H. Sherwood, C. T. Rettner, K. Ohno, D. D. Awschalom, and D. Rugar, Science **339**, 557 (2013).

[21] T. Staudacher, F. Shi, S. Pezzagna, J. Meijer, J. Du, C. A. Meriles, F. Reinhard, and J. Wrachtrup, Science **339**, 561 (2013).

[22] M. Loretz, S. Pezzagna, J. Meijer, and C. L. Degen, Appl. Phys. Lett. **104**, 033102 (2014).

[23] L. J. Su, C. Y. Fang, Y. T. Chang, K. M. Chen, Y. C. Yu, J. H. Hsu, and H. C. Chang, Nanotechnology **24**, 315702 (2013).

[24] W. Kaiser and W. L. Bond, Phys. Rev. **115**, 857 (1959).

[25] W. V. Smith, P. P. Sorokin, I. L. Gelles, and G. J. Lasher, Phys. Rev. **115**, 1546 (1959).

[26] M. W. Doherty, N. B. Manson, P. Delaney, F. Jelezko, J. Wrachtrup, and L. C. Hollenberg, Phys. Rep. **528**, 1 (2013).

[27] A. Henstra and W. T. Wenckebach, Mol. Phys. **112**, 1761 (2014).

[28] U. L. Gunther, Top. Curr. Chem. **335**, 23 (2013).

[29] D. E. J. Waddington, M. Sarracanie, H. Zhang, N. Salameh, D. R. Glenn, E. Rej, T. Gaebel, T. Boele, R. L. Walsworth, D. J. Reilly, and M. S. Rosen, arXiv:1611.05167.

[30] G. A. Rinard and G. R. Eaton, Loop-gap resonators, in *Biomedical EPR, Part B: Methodology, Instrumentation, and Dynamics*, edited by S. R. Eaton, G. R. Eaton, and L. J. Berliner (Springer, Boston, 2005), pp. 19–52.

[31] K. Chen, W. Liu, Y. Feng, and W. Li, J. Phys. E **21**, 660 (1988).

[32] See Supplemental Material at http://link.aps.org/supplemental/10.1103/PhysRevB.95.064413 for orientation of the diamond chip in the EPR setup (Fig. S1), experimental EPR spectra at X-band (Fig. S2), calculated EPR spectrum at 51 mT (Fig. S3), and simulated NV and P1 populations (Fig. S4).

[33] V. M. Acosta, E. Bauch, M. P. Ledbetter, C. Santori, K. M. C. Fu, P. E. Barclay, R. G. Beausoleil, H. Linget, J. F. Roch, F. Treussart, S. Chemerisov, W. Gawlik, and D. Budker, Phys. Rev. B **80**, 115202 (2009).

[34] T. L. Wee, Y. K. Tzeng, C. C. Han, H. C. Chang, W. Fann, J. H. Hsu, K. M. Chen, and Y. C. Yu, J. Phys. Chem. A **111**, 9379 (2007).

[35] A. Jarmola, V. M. Acosta, K. Jensen, S. Chemerisov, and D. Budker, Phys. Rev. Lett. **108**, 197601 (2012).

[36] X. D. Chen, L. M. Zhou, C. L. Zou, C. C. Li, Y. Dong, F. W. Sun, and G. C. Guo, Phys. Rev. B **92**, 104301 (2015).

[37] N. B. Manson and J. P. Harrison, Diamond Relat. Mater. **14**, 1705 (2005).

[38] N. Aslam, G. Waldherr, P. Neumann, F. Jelezko, and J. Wrachtrup, New J. Phys. **15**, 013064 (2013).

[39] E. Bourgeois, A. Jarmola, P. Siyushev, M. Gulka, J. Hruby, F. Jelezko, D. Budker, and M. Nesladek, Nat. Commun. **6**, 8577 (2015).

[40] F. J. Heremans, G. D. Fuchs, C. F. Wang, R. Hanson, and D. D. Awschalom, Appl. Phys. Lett. **94**, 152102 (2009).

[41] H. Jayakumar, J. Henshaw, S. Dhomkar, D. Pagliero, A. Laraoui, N. B. Manson, R. Albu, M. W. Doherty, and C. A. Meriles, Nat. Commun. **7**, 12660 (2016).

[42] E. C. Reynhardt, G. L. High, and J. A. V. Wyk, J. Chem. Phys. **109**, 8471 (1998).

[43] P. Deak, B. Aradi, M. Kaviani, T. Frauenheim, and A. Gali, Phys. Rev. B **89**, 075203 (2014).

[44] J. Chen, S. Lourette, K. Rezai, T. Hoelzer, M. Lake, M. Nesladek, L. S. Bouchard, P. Hemmer, and D. Budker, arXiv:1607.08354.